PERFORMANCE OF THE CRYPTOSTEADY-FLOW ENERGY SEPARATOR

Joseph V. Foa

George Washington University

Prepared for:

Naval Air Systems Command

July 1972

TR-ES-722
July 1972

PERFORMANCE OF THE CRYPTOSTEADY-FLOW ENERGY SEPARATOR

by

Joseph V. Foa

School of Engineering and Applied Science
The George Washington University
Washington, D.C. 20006

r

ACKNOWLEDGMENT

This work was supported by the Mechanical Equipment Branch of the U. S. Naval Air Systems Command, under Contract Number N00019-72-C-0122.

ABSTRACT

Performance equations are developed for the cryptosteady-flow energy separator in its most general form and over the widest range of operating conditions considered so far, including bearing friction or other rotor torque, and unequal discharge pressures, peripheral velocities, flow losses, prerotation velocities, and discharge angles.

Equations are also developed for the proportioning of rotor nozzles in accordance with performance specifications.

Convenient performance and design charts are also presented.

NOMENCLATURE

$\vec{c}$ = fluid particle velocity in F_s

F_s = frame of reference in which the flow is steady

F_u = frame of reference in which the energy separation is utilized

h = specific static enthalpy

h° = specific stagnation enthalpy in F_u

h^* = specific stagnation enthalpy in F_s

L = externally-applied rotor torque (positive if driving torque)

$\dot{m}$ = mass flow rate

M = Mach number

p = static pressure

p° = stagnation pressure in F_u

$\vec{u}$ = fluid particle velocity in F_u

$\vec{u}'$ = "prerotation" velocity

$\vec{V}$ = velocity of F_s relative to F_u

α = ratio of total nozzle exit area on b side to total nozzle exit area on a side

β = inclination of nozzle axis to normal to $\vec{V}$ in external-separation devices (see Fig. 2)

γ = ratio of specific heats

δ = cos θ (negative on a side)

η = $(h^* - h_d)/(h^* - h_o)$ (nozzle efficiency)†

θ = angle $(\vec{V},\vec{c})$

---

†Note that this definition differs from those used in previous papers on this subject.

κ = $\dot{m}_a(h_i^\circ - h_a^\circ)/\dot{m}_i V_a^2$ (cooling capacity coefficient)

λ = p_d^*/p_i^*

μ = $\dot{m}_b/\dot{m}_a$ (mass flow ratio)

ν = $\dot{m}_a/\dot{m}_i$ (cold fraction)

ρ = density

ω = angular velocity of the rotor

Subscripts

a = flow discharged with $\delta < 0$

b = flow discharged with $\delta \geq 0$

d = rotor nozzle discharge

e = rotor nozzle entrance

i = energy separator input flow

o = conditions resulting from isentropic discharge from p_i° to p_d. For example,
$u_{oa}^2 = 2h_i^\circ \left[1-(p_{da}/p_i^\circ)^{\frac{\gamma-1}{\gamma}}\right]$

Superscripts

o = stagnation quantities in F_u

* = stagnation quantities in F_s

Assumptions

(1) The fluid, when compressible, is assumed to be a calorically perfect gas.
(2) In external-separation configurations, the radial distance between rotor and stator is small compared to the rotor radi
(3) Heat exchanges with the surroundings, in the energy separator, are negligible.
(4) Prerotation velocities are everywhere parallel to $\vec{V}$.

INTRODUCTION

Cryptosteady energy separation is a process whereby the total head or total specific enthalpy of a portion of a flow is increased at the expense of the corresponding quantities in the remainder of the same flow, through direct and essentially non-dissipative exchanges of energy.

It is known that reversible transfers of mechanical energy in flow systems are possible only where the interacting flows are nonsteady [1][1]. Indeed, in the only known steady-flow mechanism of redistribution of energy within an initially homogeneous flow--that of the Ranque-Hilsch tube [2,3]--the transfer of energy is effected, rather inefficiently, through the action of viscous stresses. On the other hand, considerably better performance has been shown to be possible when the energy transfer is effected by "pressure exchange," i.e., through the work of interface pressure forces; and pressure exchange is always a nonsteady process, because no work is done by pressure forces acting on a stationary interface.

In an effort to improve energy separator performance through the utilization of pressure exchange, some attention has been given during the last decade to devices called "dividers," which operate on the basis of wave processes [4,5]. There is reason to believe, however, that the development of practical and efficient dividers would be very difficult, because of the sensitivity of these devices to such factors as imperfect timing of moving mechanical parts to wave and flow processes, diffusion of

[1]Numbers in brackets designate References at end of paper.

interfaces, noninstantaneous opening and closing of valves, distortion of shock fronts, etc., not to mention the usual analytical complexities of nonsteady-flow processes.

This paper deals with a nonsteady-flow method of energy separation in which the difficulties just mentioned are overcome through the utilization of "cryptosteady" pressure exchange--a cryptosteady process being defined as one that is nonsteady but admits a frame of reference in which it is steady. The special merit of cryptosteady processes is that they can be generated, controlled, and analyzed as steady-flow processes in this unique frame of reference, while retaining all the potential advantages of nonsteady flows in the frame of reference in which they are utilized.

A simple interaction of this type is shown in Fig. 1. Here two flows deflect each other to a common orientation in a frame of reference F_s in which they are both steady. Apart from transport processes, no energy is exchanged between the two flows in this frame of reference. A transfer of energy does, however, take place--by pressure exchange--in the frame of reference F of an observer O moving at an arbitrary velocity $\vec{V}$ relative to F_s. The energy so transferred is equal to the work done by the pressure forces which the interacting flows exert on one another at their interface. This work is zero in F_s, where the interface is stationary, but not in F, where the interface moves. Since changes of the frame of observation are reversible, these energy exchanges are essentially nondissipative. Note that, because

of the existence of a frame of observation in which the flow is steady (frame F_s), the flow in F is cryptosteady. Analyses of cryptosteady interactions and discussions of some of their applications have been presented in previous papers [6,7,8,9,10].

The operation of the cryptosteady energy separator may be explained in a similar manner [11], through consideration of a simple two-dimensional situation, such as that shown in Fig. 2. Here a plane and initially homogeneous stream i is seen issuing from a nozzle as a jet and impinging on a wall W. The flow field is stationary in a frame of reference F_s, which is the coordinate system fixed to the nozzle. Body forces are assumed to be absent, and viscous stresses and heat exchanges with the surroundings are assumed to be negligible.

The impingement causes the jet to divide into two separate streams a and b, interfacing with one another at the stagnation stream surface s. For example, if the discharge pressure is the same on the two sides, the ratio of the mass flow rates in the two streams is $\mu = (1- \sin \beta)/(1+ \sin \beta)$.

The specific stagnation enthalpy (or the total head, if the fluid is incompressible) is, in frame F_s, the same in the deflected flows as in the original stream. This, however, is not true in any other frame of reference. In particular, letting $\vec{c}$ and $\vec{u}$ denote fluid particle velocities relative to F_s and to the frame of reference F_u of an observer moving relative to F_s at an arbitrary velocity $\vec{V}$ relative to the wall, respectively, one has $\vec{u} = \vec{c} + \vec{V}$, hence

$$\frac{1}{2}(u_b^2 - u_a^2) = \frac{1}{2}(c_b^2 - c_a^2) + (\vec{c}_b - \vec{c}_a)\cdot\vec{V}$$

So long as $\vec{V} \neq 0$, the term $(\vec{c}_b - \vec{c}_a)\cdot\vec{V}$ never vanishes, because $\vec{c}_b$ and $\vec{c}_a$ have different orientations. Therefore, $\frac{1}{2}(u_b^2 - u_a^2) \neq \frac{1}{2}(c_b^2 - c_a^2)$, and since the thermodynamic states are invariant with respect to changes of the frame of reference, there follows

$$h_b^o - h_a^o \neq h_b^* - h_a^*$$

Thus, if $h_b^* = h_a^*$, $h_b^o \neq h_a^o$. Since the original stream $\underline{i}$ is seen as a homogeneous stream in every coordinate system, it must be concluded that energy is transferred, in F_u, from one portion to the other of this stream, as these two portions are deflected to different orientations. This fact can also be explained on the basis of the observation that in frame F_u the interface $\underline{s}$ is moving and the interface pressure forces are therefore doing work. The energy that is transferred from $\underline{a}$ to $\underline{b}$ is, of course, the work done by $\underline{a}$ on $\underline{b}$ in this pressure exchange interaction.

As pointed out in references [11] and [12], a situation approximating that of Fig. 2 may be obtained, with a stream of finite transverse dimensions, through lateral confinement of the deflection region by means of end plates or vanes. These vanes must be shaped to lead the deflected flows into separate spaces. As a consequence, the flow can be strictly cryptosteady only if the confining vanes are stationary in F_s.

The motion of F_s relative to F_w is most simply maintained by the reaction of the issuing jet itself. In the situation of Fig. 2, the source may be a nozzle which is constrained to move in a direction parallel to the wall W. A more practical arrangement is that of Fig. 3, where jets issuing from slanted nozzles or slots on the surface of a free-spinning rotor impinge on the internal surface of an enshrouding wall. This arrangement approximates that of Fig. 2, so long as the radial depth of the annular impingement-deflection space is small compared to its mean radius.

In contrast to the "external separation" configuration of Fig. 3 (where the separation of the two flows takes place outside the rotor), Fig. 4 shows an "internal separation" arrangement. Here the separation of the two flows takes place inside the rotor. The two flows are discharged through separate nozzles, of which only two are shown. A schematic view of another internal-separation arrangement, defining some of the nomenclature used in this paper, is shown in Fig. 5. In either case, say for simplicity that bearing friction is negligible, the discharge pressure is uniform, the nozzle inclinations to the rotor surface are equal and opposite, and the internal flow losses are the same for both flows. Then, if the nozzle areas are unequal, the rotor will rotate at the angular velocity which is required for the conservation of the total angular momentum of the flow in the laboratory frame of reference (frame F_w), thus producing the required motion of F_s relative to F_w.

Several variations of these arrangements are described in reference [12].

Cryptosteady energy separation was first proposed and analyzed in reference [11], which also contains an account of some of the experiments in which the validity of the concept was first tested and confirmed.

The analysis of reference [11] accounts for most of the pertinent parameters, including rotor torque and flow losses, but covers only situations in which the peripheral velocity, the discharge pressure, and the entropy rise are the same on the b as on the a side, the inclinations of the discharge velocities on the two sides are equal and opposite, and prerotation of the input flow is absent. The effects of departures from such symmetries have received relatively little attention until recently, except for a study by Hashem [13] on the effect of prerotation and for a series of performance analyses of internal-separation devices, in which the effects of prerotation (assumed to be uniform throughout the input flow) and of differences of nozzle inclination, peripheral velocity, and discharge pressure on the two sides have been individually examined by this writer.

A more comprehensive study of the subject has recently been completed by Graham [14], as part of a comparative analysis of the three classes of energy separation techniques--steady, nonsteady, and cryptosteady. In dealing with the latter technique, the Graham paper analyzes in detail the effect of unequal pressures on the behavior of the emerging jet in external-separation

/-

devices and also examines two output flow collection effects which are critical with these devices. Viscous reattachment of the deflected jets to the collector walls is found to be potentially beneficial, whereas flow pulsations--i.e., departures from cryptosteadiness--in the collection process, resulting from the use of confining vanes stationary in F_u, are found to be detrimental. The latter determination is of particular importance, in that it provides, for the first time, a firm rationale for focussing attention on those devices of this class in which the flow is truly cryptosteady.

For such devices, whether they be of the internal- or of the external-separation variety, the Graham analysis develops "core performance" equations in which the most important design and operational parameters appear simultaneously, with full account of their nonlinear interactions. However, these equations require iterative solution in most cases, and their use is again limited in practice, because of their great complexity, to the individual evaluation of the separate effects of prerotation (again assumed to be uniform), rotor torque, and unequal back pressures, nozzle efficiencies, and exit flow orientations.

The present analysis approaches the same problem, for strictly cryptosteady situations, by a different route, which leads to simple, closed-form solutions in all cases. The analysis accounts for all design and operational parameters so far identified, as well as for their conceivable asymmetries (including unequal prerotations) and nonlinear interactions. Equations are also

developed for the design of cryptosteady-flow energy separators in accordance with any given set of feasible performance specifications.

GENERALIZED PERFORMANCE ANALYSIS

The following equations apply to both flows a and b:

$$h_d^* = h_i^\circ - \frac{u'^2}{2} + \frac{(u'-V)^2}{2}$$

$$= h_i^\circ + \frac{V^2}{2} - u'V \qquad (1)$$

and

$$c_d^2 = 2(h_d^* - h_d)$$

$$= 2\eta\left(h_d^* - h_i^\circ + \frac{u_o^2}{2}\right) \qquad (2)$$

with

$$u_o^2 = 2h_i^\circ \left[1 - \left(\frac{p_d}{p_i^\circ}\right)^{\frac{\gamma-1}{\gamma}}\right] \qquad (3)$$

Equation (3) is plotted, for $\gamma = 1.40$, in Figure 6.

From Equations (1) and (2) there follows

$$c_d^2 = \eta(V^2 - 2u'V + u_o^2) \qquad (4)$$

Equation (4) is plotted in Figure 7.

Also,

$$u_d^2 = c_d^2 + V^2 + 2c_d V\delta \qquad (5)$$

and, by definition,

$$h_d^\circ - h_d^* = \frac{1}{2}(u_d^2 - c^2) \qquad (6)$$

Equations (1), (4), (5), and (6) yield

$$h_d^\circ - h_i^\circ = V^2 + \delta V\left[\eta\left(u_o^2 + V^2 - 2u'V\right)\right]^{1/2} - u'V \qquad (7)$$

Thus,

$$\frac{h_i^\circ - h_a^\circ}{V_a^2} = \frac{u'_a}{V_a} - 1 - \delta_a\left[\eta_a\left(\frac{u_{oa}^2}{V_a^2} + 1 - 2\,\frac{u'_a}{V_a}\right)\right]^{1/2} \qquad (8)$$

$$\frac{h_b^\circ - h_i^\circ}{V_b^2} = 1 - \frac{u'_b}{V_b} + \delta_b\left[\eta_b\left(\frac{u_{ob}^2}{V_b^2} + 1 - 2\,\frac{u'_b}{V_b}\right)\right]^{1/2} \qquad (9)$$

The use of V as an independent variable is analytically convenient (as shown by the development above) and is justified by the specific constraints to which the selection of this parameter is subjected in practice (constraints of rotor size and structural strength, of bearing characteristics, etc.).

Equations (8) and (9) cover the greatest variety of configurations and operating conditions so far considered, including such asymmetries as unequal peripheral velocities, discharge pressures, flow prerotation velocities, and discharge angles. Rotor speed is implicitly accounted for through the mass flow ratio, as will be seen below and under DESIGN EQUATIONS.

The mass flow ratio is related to the specific enthalpy increments through the energy equation

$$\dot{m}_a h_a^\circ + \dot{m}_b h_b^\circ = \dot{m}_i h_i^\circ + L\omega$$

whence

$$\mu = \frac{h_i^\circ - h_b^\circ + \dfrac{L\omega}{\dot{m}_i}}{h_a^\circ - h_b^\circ - \dfrac{L\omega}{\dot{m}_i}} \qquad (10)$$

The "cold fraction" is

$$\nu = \frac{1}{1+\mu} \tag{11}$$

and the "cooling capacity coefficient" is, by definition,

$$\kappa = \nu(h_i^\circ - h_a^\circ)/V_a^2 \tag{12}$$

Equations (8) and (9) are plotted, for $\gamma = 1.40$, in Figs. 8(a) through 8(p). These two equations are uncoupled, in the sense that the stagnation enthalpy increments on the a and b sides can be obtained separately from them or from the charts. Fig 8(a) illustrates the use of the charts for a case in which the two stagnation enthalpy increments can be read on the same chart because $\delta_b = -\delta_a$ and $\eta_b = \eta_a$. The example chosen is that of an energy separator in which $\delta_b = -\delta_a = 0.95$ and $\eta_a = \eta_b = 0.90$, operating at prescribed nozzle-exit peripheral velocities V_a and V_b, with prerotation velocities $u'_a = 0.5V_a$ and $u'_b = -0.435V_b$, and under such pressures p_i°, p_{da} and p_{db} that u_{oa} and u_{ob} -- as obtained from Eq. (3) or from Fig. 6 -- are equal to $4V_a$ and $4V_b$, respectively. To obtain the stagnation enthalpy drop on the a side, enter the prescribed value of u'_a/V_a on the pertinent scale (point A), read down vertically to the curve for $u_{oa}/V_a = 4$ (point B) and then horizontally to the $(h_i^\circ - h_a^\circ)/V_a^2$ scale for the sought information (point C). The stagnation enthalpy rise on the b side is similarly obtained by entering the known value of u'_b/V_b on the pertinent scale (point D), and proceeding from there horizontally to the curve for the

appropriate value of u_{ob}/V_b (point E), and thence vertically for the sought reading at F. If $\delta_b \neq -\delta_a$ and/or $\eta_b \neq \eta_a$, the readings C and F must be obtained separately, each from the appropriate chart. The corresponding value of μ is obtained from Eq. (10). If rotor torque is absent or negligible, and if the two readings C and F are transposed to the same chart, the value of μ is that which pertains to the radial line through point G, whose coordinates are the two readings C and F. In the case of the illustrative example of Fig. 8(a) $\mu = 0.6\ V_a^2/V_b^2$. Fig. 9 is a convenient chart for the comparative evaluation of solutions from the standpoint of cooling capacity, for situations in which rotor torque is negligible and $V_a = V_b$.

Figs. 6 through 9 can be used, of course, also in the solution of the reverse problems resulting from interchanges of dependent and independent variables (e.g., in the determination of the rotor speed and input and discharge pressures that are required to produce a specified cooling capacity coefficient). Furthermore, visual inspection of these charts readily uncovers a good deal of useful information on the magnitude, sizes, and relative importance of changes of various parameters in relation to their separate or combined effects on performance. Thus, for example, the charts confirm the existence of an optimum positive prerotation on the a side when the pressure ratio on that side is low; they reveal that opposite prerotations--positive on the a side and negative on the b side--can be remarkably beneficial from the standpoint of cooling capacity for any given rotor speed; and

they provide a tool for the quick selection of the operational parameters that will best combine to produce any desired result.

DESIGN EQUATIONS

The equations developed in the preceding section apply, of course, to both internal- and external-separation devices. Thus, once a satisfactory solution has been identified, the determination of the combination of operational parameters (rotor speed, mass flow ratio, etc.) that will produce this solution is the same for both subgroups. The same cannot be said, however, of the manner in which the selected combination can be implemented. In the first place, in internal-separation devices the controlling design parameter is the nozzle area ratio α, whereas in external separation devices it is the impingement angle β. In the second place, the effect of unequal discharge pressures on rotor speed and mass flow ratio is markedly different in the two subgroups [14]. Finally, impingement wall boundary layer effects on performance, absent in internal separation, are believed to be potentially significant in external separation, although very little is yet known about them. The latter point is particularly important, in that it points to residual uncertainties that still make the correlation of design to performance a good deal less reliable with external than with internal separation. For this reason, only the internal-separation version will be considered here.

Two cases will be discussed:

(a) the case in which the two flows a and b are both fully expanded, within the rotor nozzles, to their respective discharge pressures p_a and p_d, and

(b) the case in which the rotor nozzles are under-expanded and both flows are sonic at the nozzle exits.

Case (a).

If the nozzle flows are fully expanded, $c_e = c_d$ on both sides. These velocities can be obtained from Eq. (4) or from Fig. 7.

From the equation of state,

$$\frac{\rho_{db}}{\rho_{da}} = \frac{p_{db}}{p_{da}} \frac{h_{da}}{h_{db}}$$

$$= \frac{p_{db}}{p_{da}} \frac{h^*_{da} - \frac{c^2_{da}}{2}}{h^*_{db} - \frac{c^2_{db}}{2}} \tag{13}$$

and, from the definition of μ,

$$\mu = \alpha \frac{c_{db}}{c_{da}} \frac{\rho_{db}}{\rho_{da}} \tag{14}$$

Finally, Eqs. (1), (13), and (14) yield

$$\alpha = \mu \frac{c_{da}}{c_{db}} \frac{p_{da}}{p_{db}} \frac{2h^\circ_i + V^2_b - 2u'_b V_b - c^2_{db}}{2h^\circ_i + V^2_a - 2u'_a V_a - c^2_{da}} \tag{15}$$

μ is calculated from Eq. (10), and it is through this parameter that rotor torque is accounted for.

Case (b).

Since $M_{ea} = M_{eb}$, the mass flow ratio is [15]

$$\mu = \alpha \frac{p^*_{eb}}{p^*_{ea}} \left(\frac{h^*_{da}}{h^*_{db}}\right)^{1/2} \tag{16}$$

17.

Now, on each side, $p_c^* = \lambda p_i^* = \lambda p_i^\circ \left(\frac{h_d^*}{h_i^\circ}\right)^{\frac{\gamma}{\gamma-1}}$. Thus,

$$\mu = \alpha \frac{\lambda_b}{\lambda_a} \left(\frac{h_{db}^*}{h_{da}^*}\right)^{\frac{\gamma+1}{2(\gamma-1)}} \tag{17}$$

Eqs. (1) and (17) yield, for $\gamma = 1.40$,

$$\alpha = \mu \frac{\lambda_a}{\lambda_b} \left(\frac{2h_i^\circ + V_a^2 - 2u_a' V_a}{2h_i^\circ + V_b^2 - 2u_b' V_b}\right)^3 \tag{18}$$

where, as before, μ is obtained from Eq. (10) and accounts for L.

SYMMETRICAL CASES

For those cases in which $\delta_b = -\delta_a$, $\eta_b = \eta_a$ (or $\lambda_b = \lambda_a$), $u_{ob} = u_{oa}$, $V_b = V_a = V$, $u_b' = u_a' = 0$, and $L = 0$, Eqs. (8) through (12), and (15) or (18), yield

$$h_b^\circ - h_i^\circ = h_i^\circ - h_a^\circ + 2V^2 \tag{19}$$

and

$$(h_i^\circ - h_a^\circ) = \mu(h_b^\circ - h_i^\circ) \tag{20}$$

hence

$$h_i^\circ - h_a^\circ = \frac{2\mu}{1-\mu} V^2 \tag{21}$$

$$\mu = \alpha \tag{22}$$

and

$$\kappa = \frac{2\mu}{1-\mu^2} \tag{23}$$

REFERENCES

1. Dean, C. R., Jr., "On the necessity of nonsteady flow in fluid machines," Trans. ASME 81, Series D, No. 1, March 1959, pp. 24-28.
2. Ranque, G. J., "Experience sur la détante giratoire avec productions simultanées d'un echappement d'air chaud et d'air froid," Journal de Physique et de Radium, 1933, p. 112.
3. Hilsch, R., "The use of the expansion of a gas in a centrifugal field as a cooling process," Review of Scientific Instruments 18, No. 2, February 1947, pp. 108-113.
4. Azoury, P. H., "An introduction to the dynamic pressure exchanger," Proceedings of the Institution of Mechanical Engineers 180, Part I, No. 18, 1965-1966, pp. 451-473.
5. Kentfield, J. A. C., "The performance of pressure-exchanger dividers and equalizers," ASME Paper No. 68-WA/FE-24, December 1968.
6. Foa, J. V., "A new method of energy exchange between flows and some of its applications," Rensselaer Polytechnic Institute Tech. Rept. TR AE 5509, December 1955.
7. Foa, J. V., "Cryptosteady pressure exchange," Rensselaer Polytechnic Institute Tech. Rept. TR AE 6202, March 1962.
8. Hohenemser, K. H., "Preliminary analysis of a new type of thrust augmenter," Proceedings of the 4th U.S. National Congress of Applied Mechanics (ASME, New York, 1962), pp. 1291-1299.

9. Foa, J. V., "A method of energy exchange," Am. Rocket Soc. J. 32, No. 9, September 1962, pp. 1396-1398.

10. Foa, J. V., "A pressure exchanger for marine propulsion," SAE Transactions 79, 1970, pp. 346-352.

11. Foa, J. V., "Energy separator," Rensselaer Polytechnic Institute Tech. Rept. TR AE 6401, January 1964.

12. U.S. Patent No. 3,361,336 (January 2, 1968).

13. Hashem, J. S., "A comparative study of steady- and nonsteady-flow energy separators," Rensselaer Polytechnic Institute Tech. Rept. TR AE 6504, October 1965.

14. Graham, P. A., "A theoretical study of fluid dynamic energy separation," The George Washington University, School of Engineering and Applied Science, Tech. Rept. TR ES 721, June 1972.

15. Foa, J. V., Flight Propulsion, Wiley, 1960, pp. 42-43.

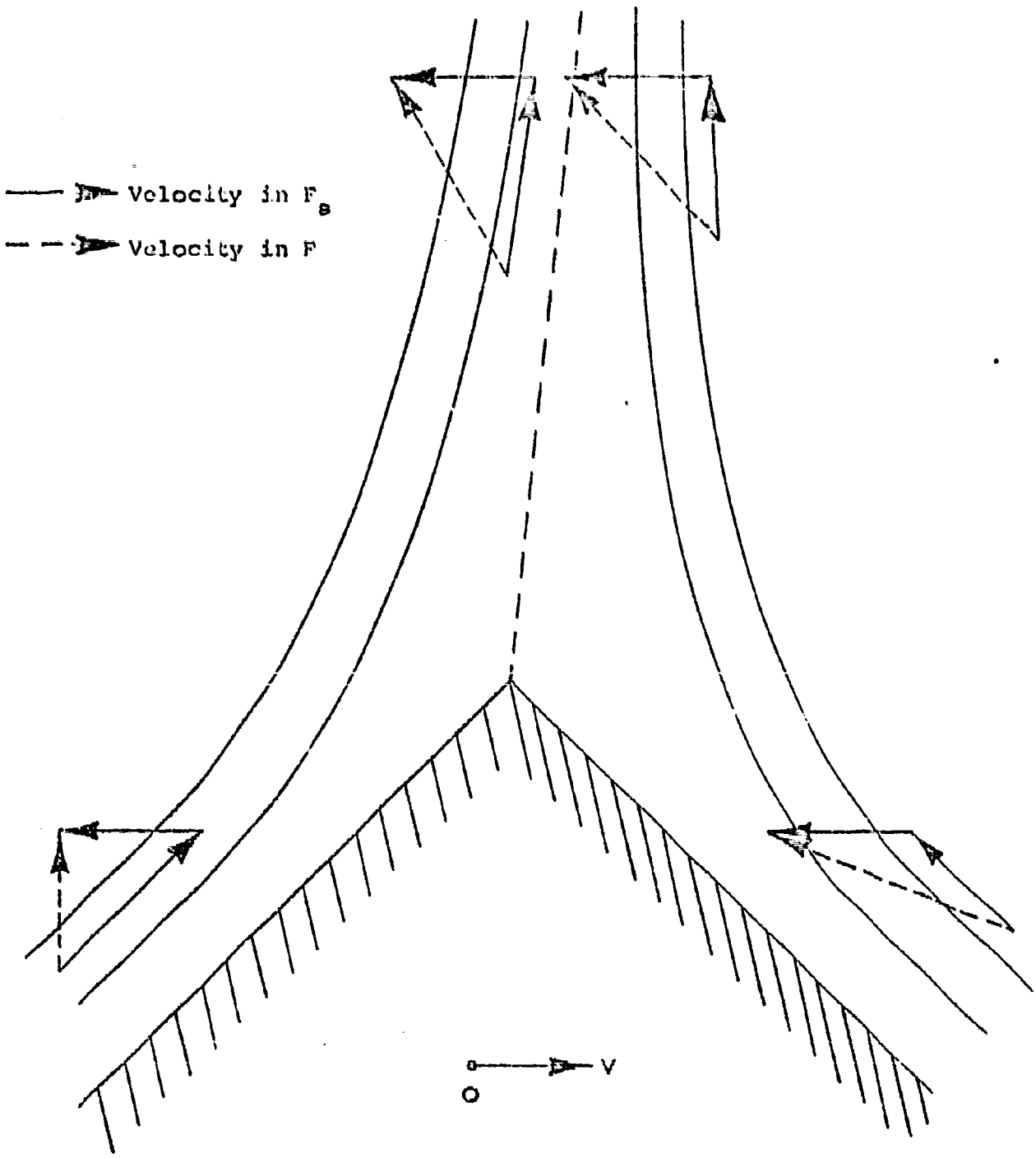

Figure 1

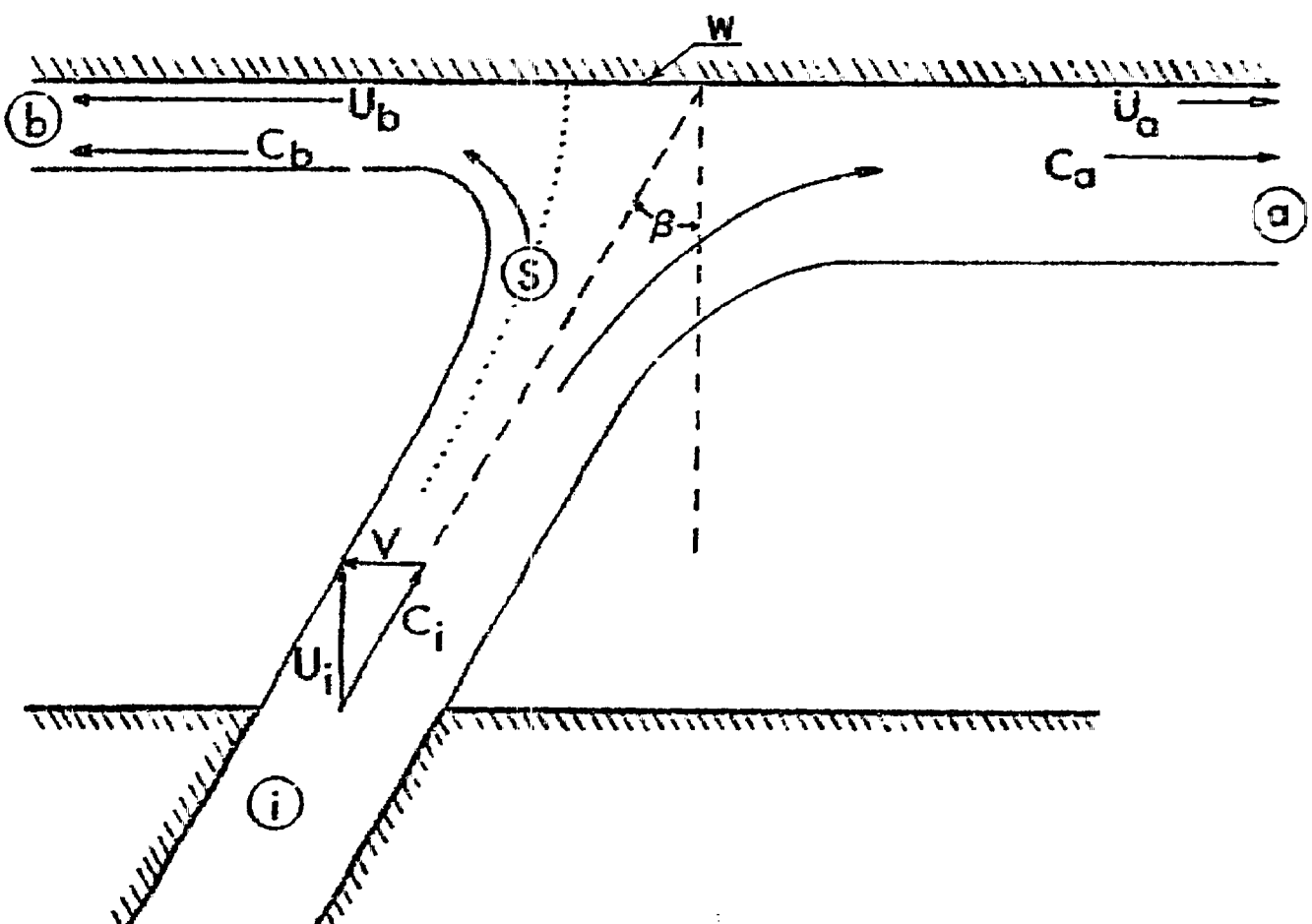

Figure 2

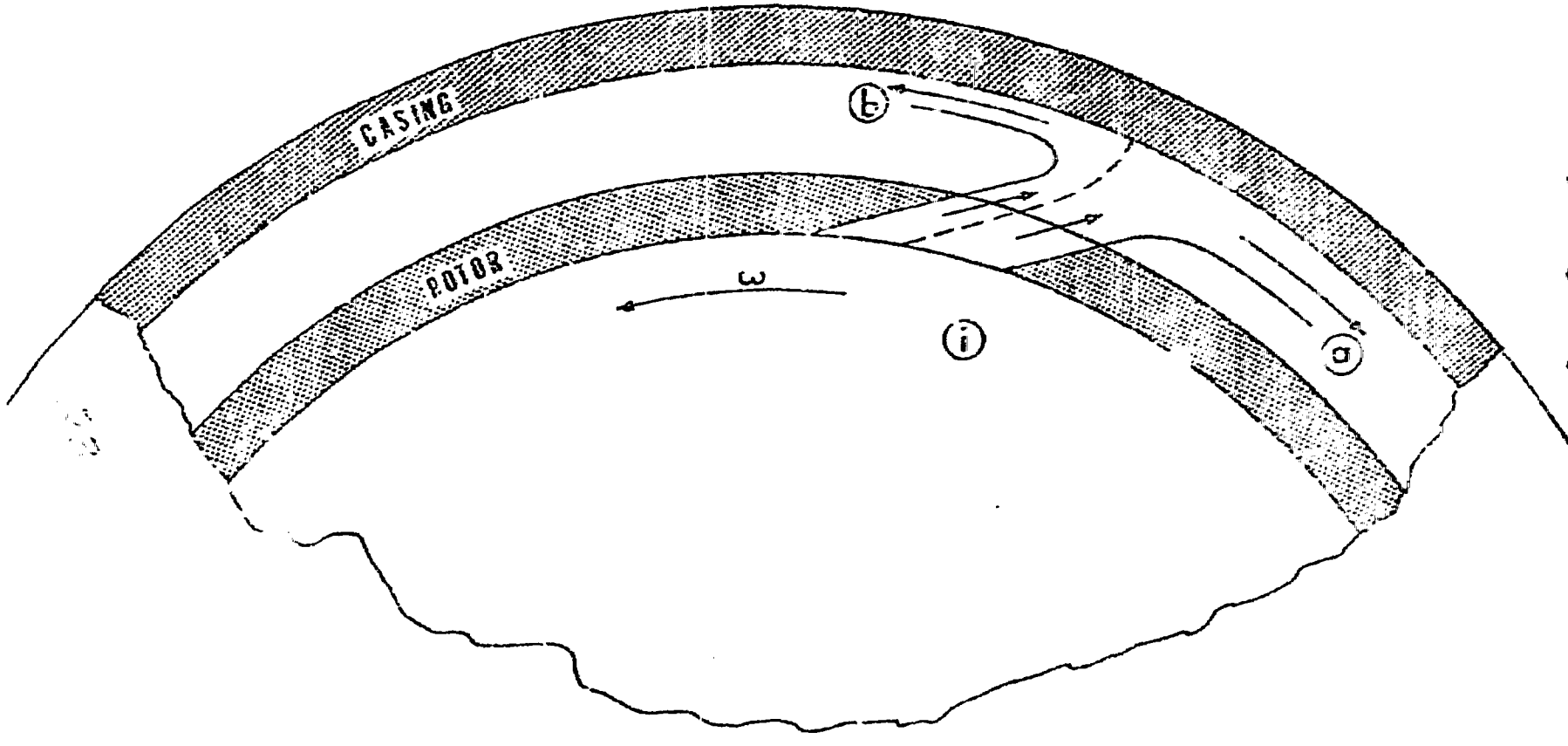

Figure 3

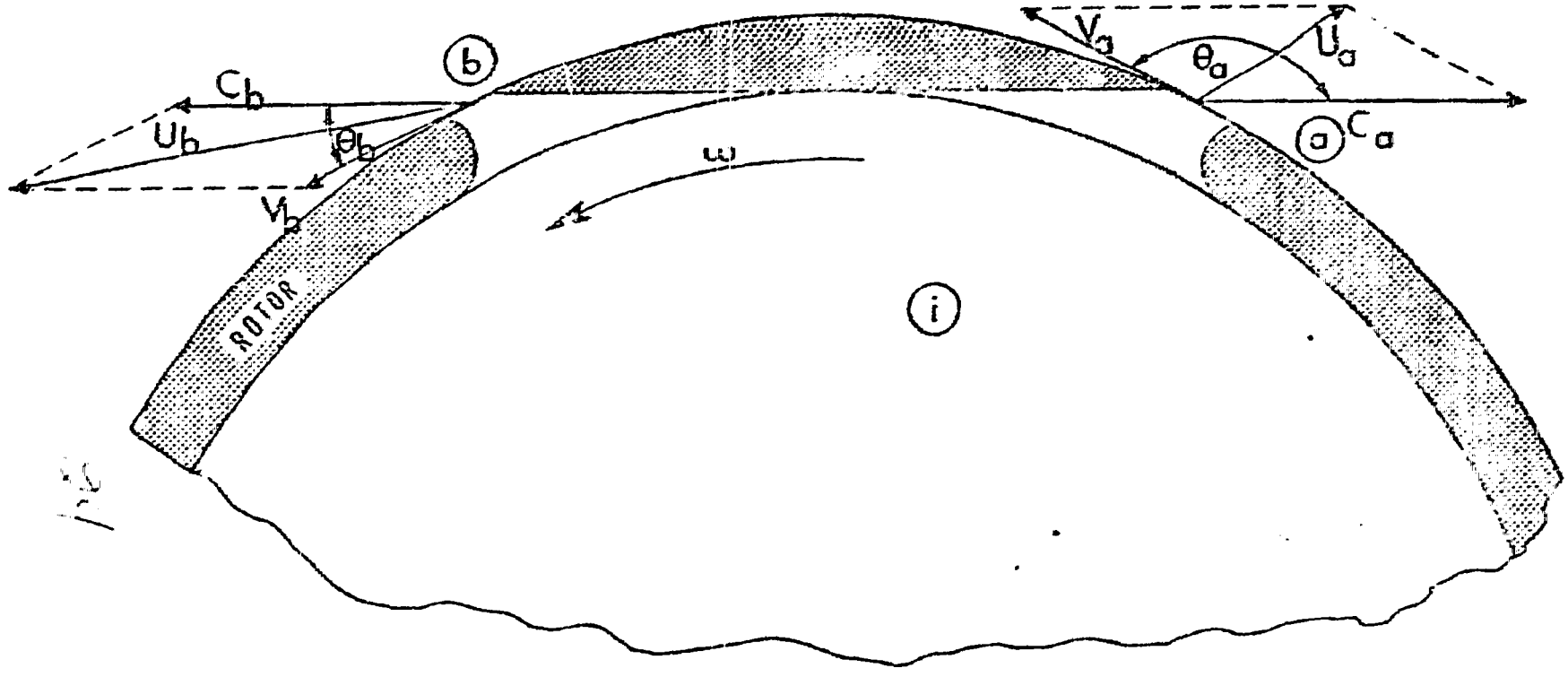

Figure 4

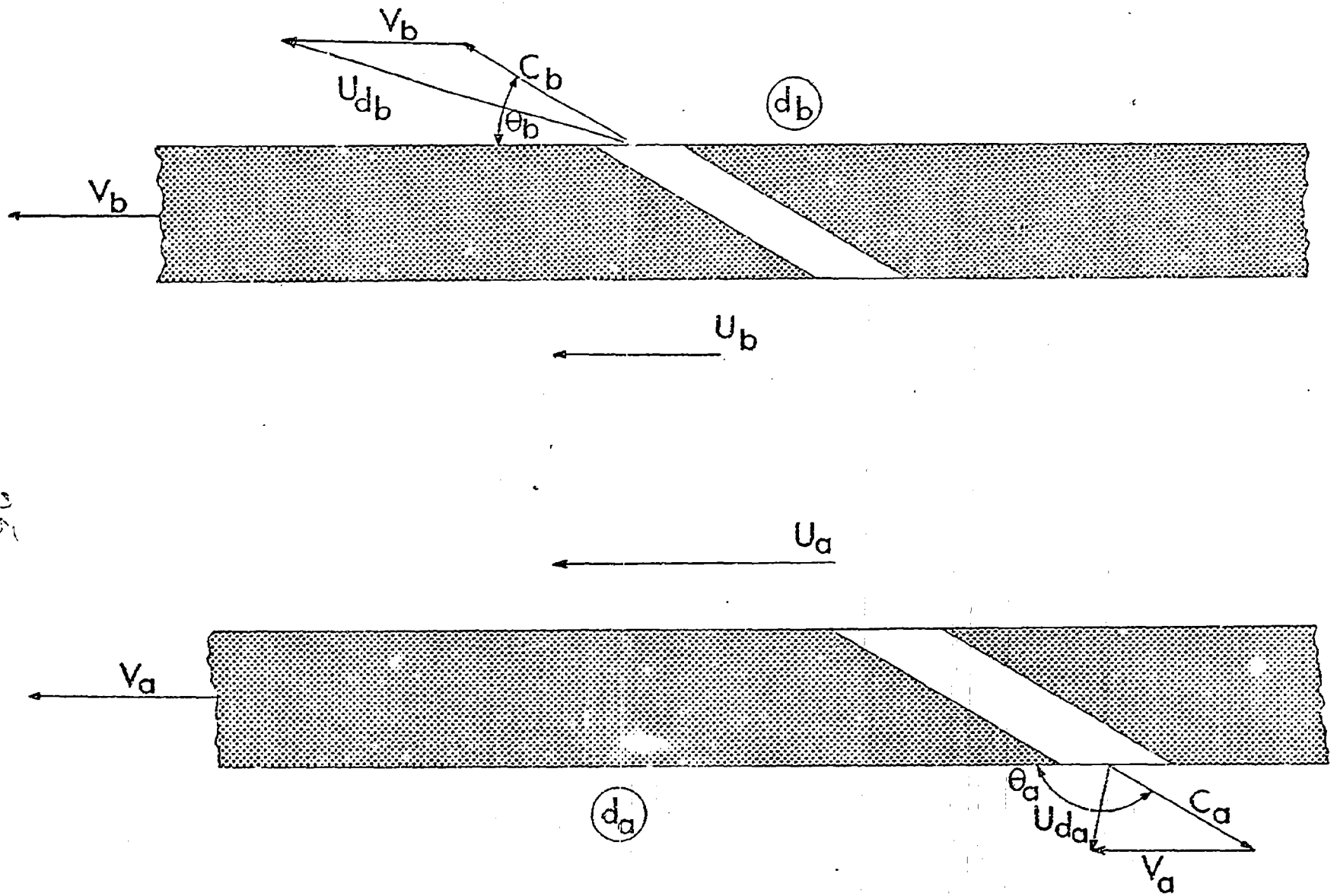

FIGURE 5

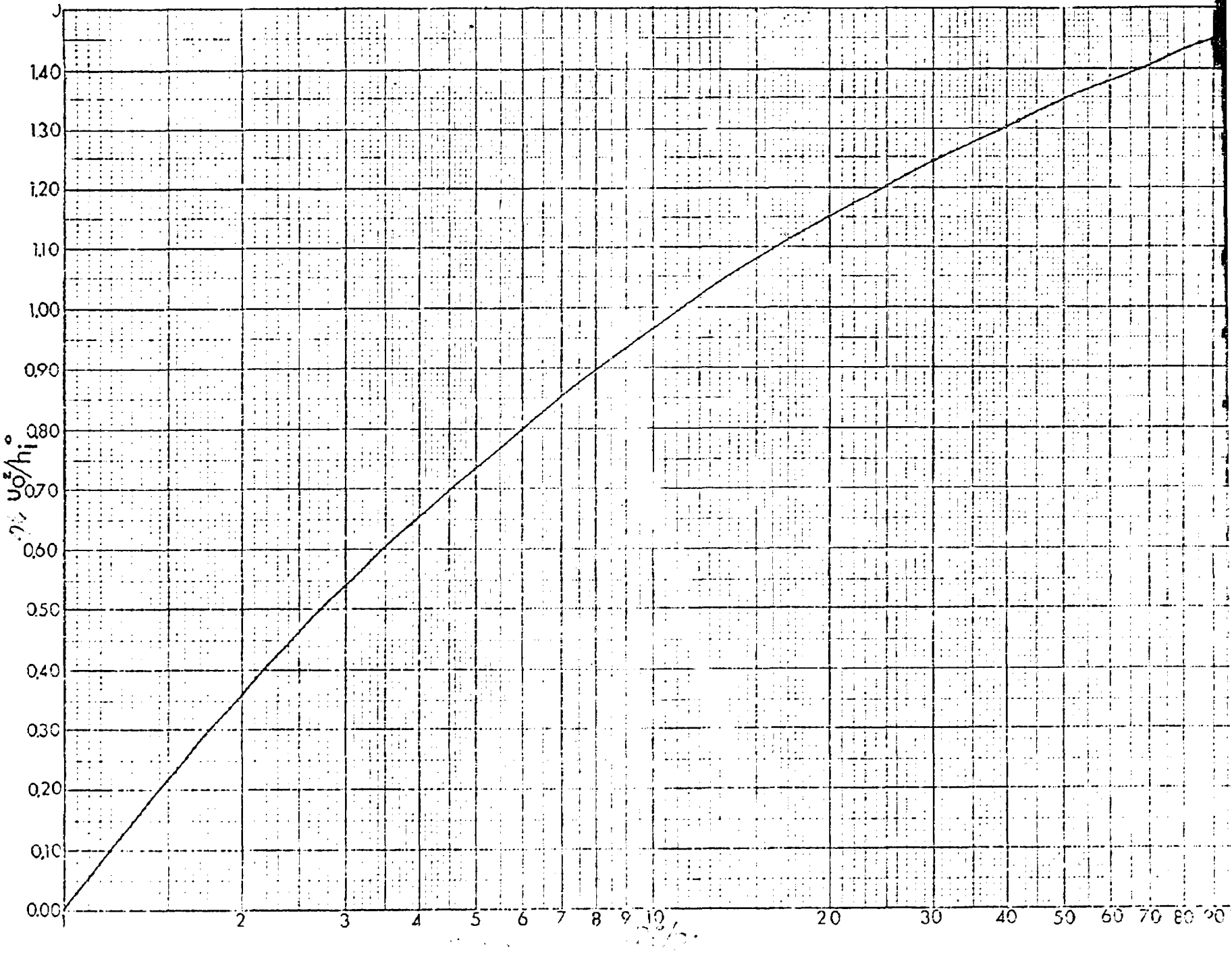
J
1.40
1.30
1.20
1.10
1.00
0.90
0.80
0.70
0.60
0.50
0.40
0.30
0.20
0.10
0.00
v_o^2/h_i
2
3
4
5
6
7
8
9
10
20
30
40
50
60
70
80
90

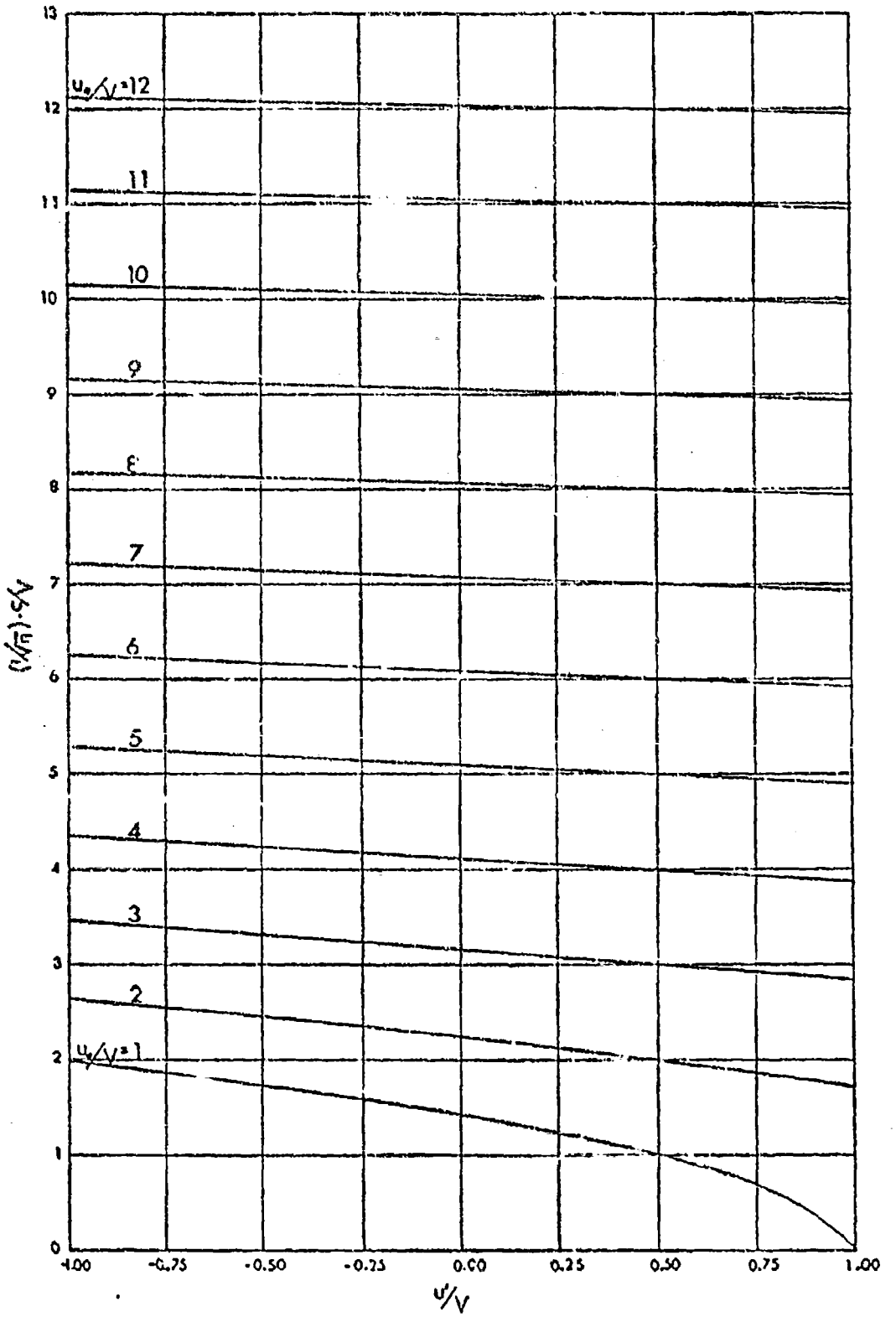
$u_0/V=12$
11
10
9
8
7
6
5
4
3
2
$u_0/V=1$
$(u/\sqrt{\pi})\cdot\sqrt{\nu}$
u'/V
-1.00
-0.75
-0.50
-0.25
0.00
0.25
0.50
0.75
1.00
0
1
2
3
4
5
6
7
8
9
10
11
12
13

Figure 7

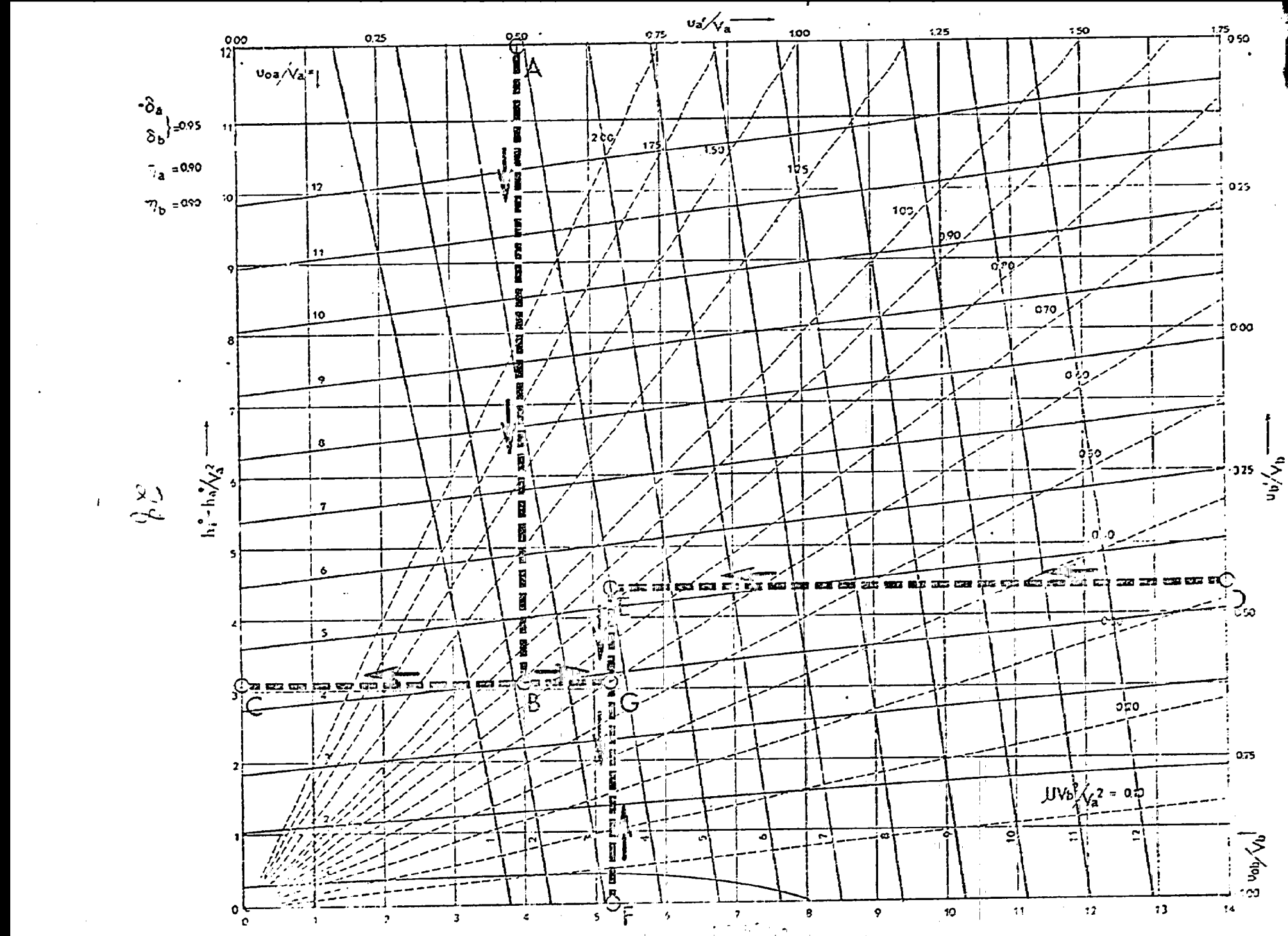
u_a'/V_a
u_{oa}/V_a
$-\delta_a$
δ_b = 0.95
η_a = 0.90
η_b = 0.90
$h_i^\circ - h_a^\circ/V_a^2$
u_b'/V_a
u_{ob}/V_a
UV_b^2/V_a^2 = 0.5
A
B
C
G

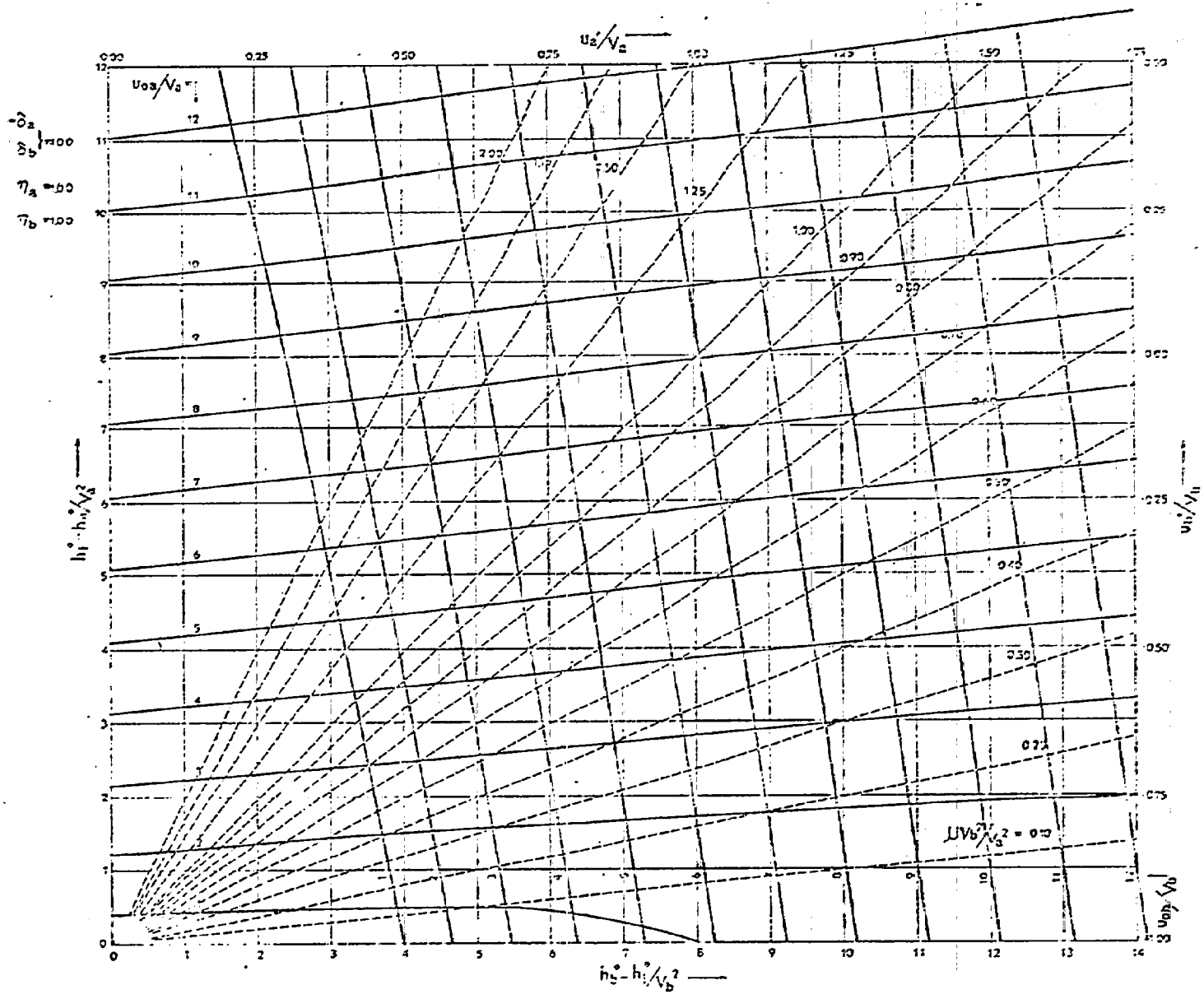
u_2/V_a
u_{03}/V_a
$-\delta_a$
δ_b
η_a
η_b
$h_1^\circ - h_{1s}^\circ/V_a^2$
$h_2^\circ - h_1^\circ/V_b^2$
u_{1s}/V_a
u_{03}/V_b
$\mu V_b^2/V_a^2 = 0.10$

FIGURE 8 (b)

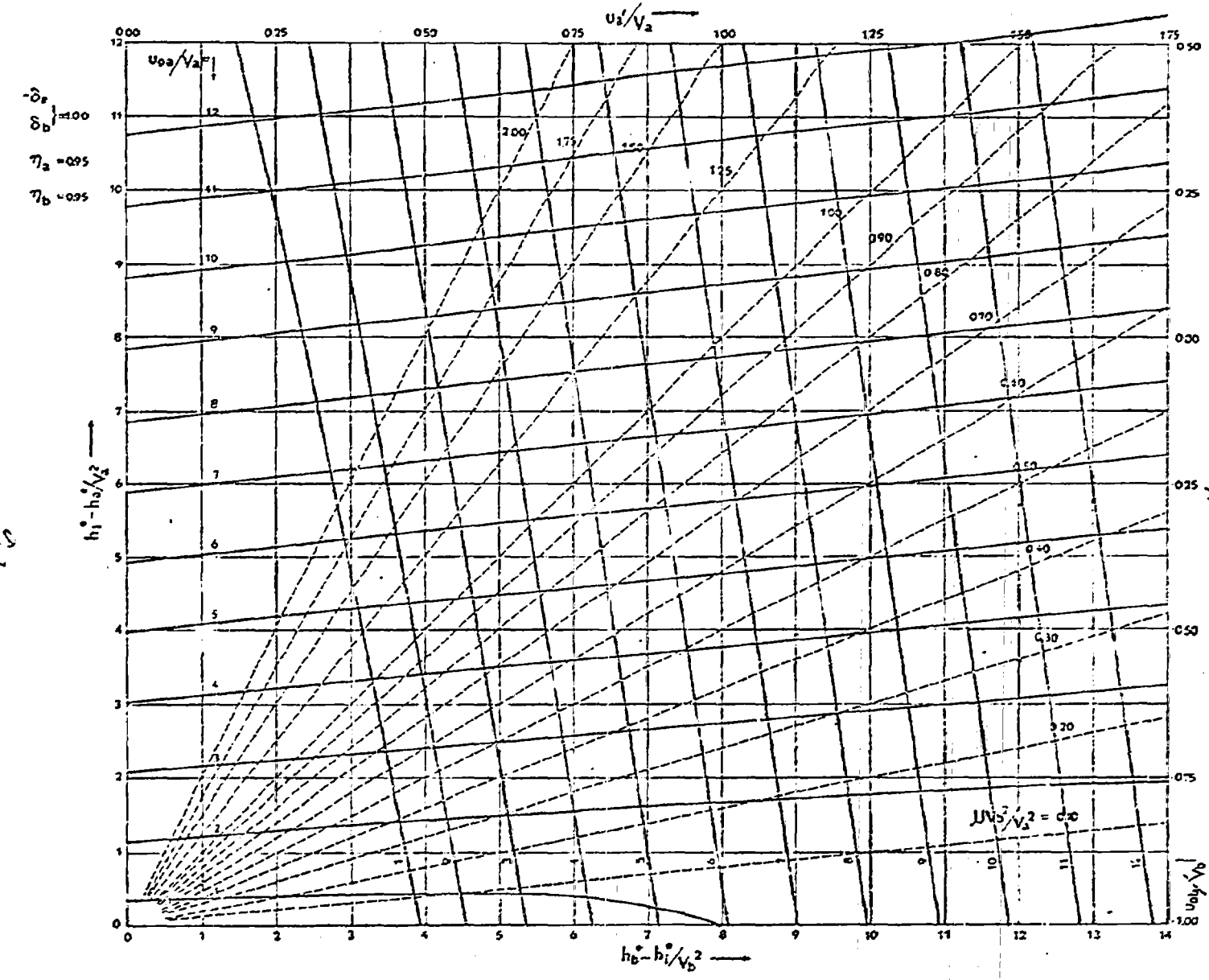
u_2'/V_2
u_{oa}/V_a
$-\delta_a$
δ_b
η_a =0.95
η_b =0.95
$h_1^*-h_a^*/V_a^2$
$h_b^*-h_1^*/V_b^2$
u_1'/V_b
u_{ob}/V_b
JN_b^2/V_a^2 = 0.30

FIGURE 8 (c)

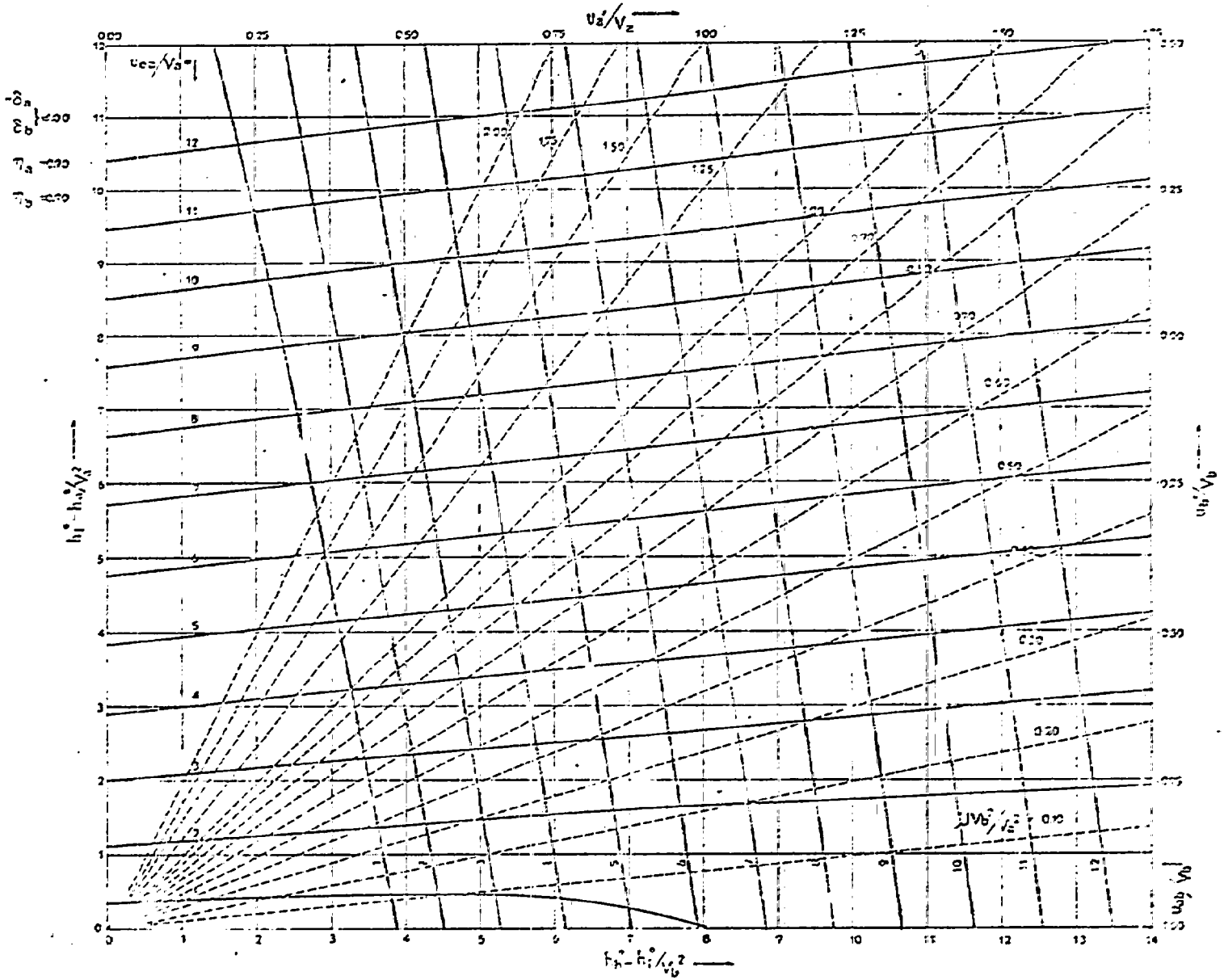

FIGURE 8(d)

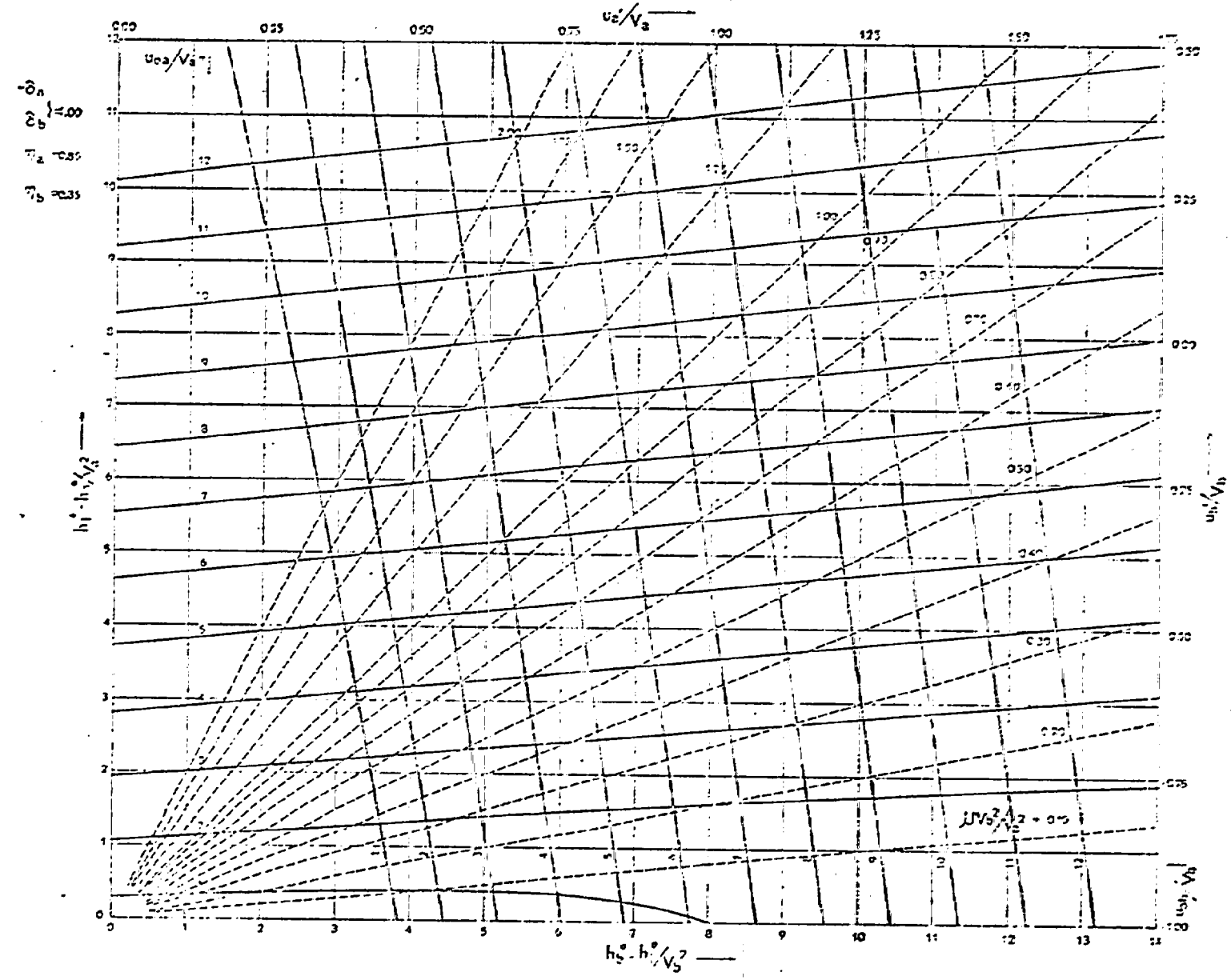
u_2'/V_a
u_{2a}/V_a
$-\delta_n$
$\hat{\epsilon}_b$ =.00
η_a =.85
η_b =.85
$h_1^* - h_1^*/V_a^2$
$h_3^* - h_3^*/V_3^2$
u_{3h}'/V_b
$\mu V_3^2/V_2^2$ = .05

FIGURE 8(a)

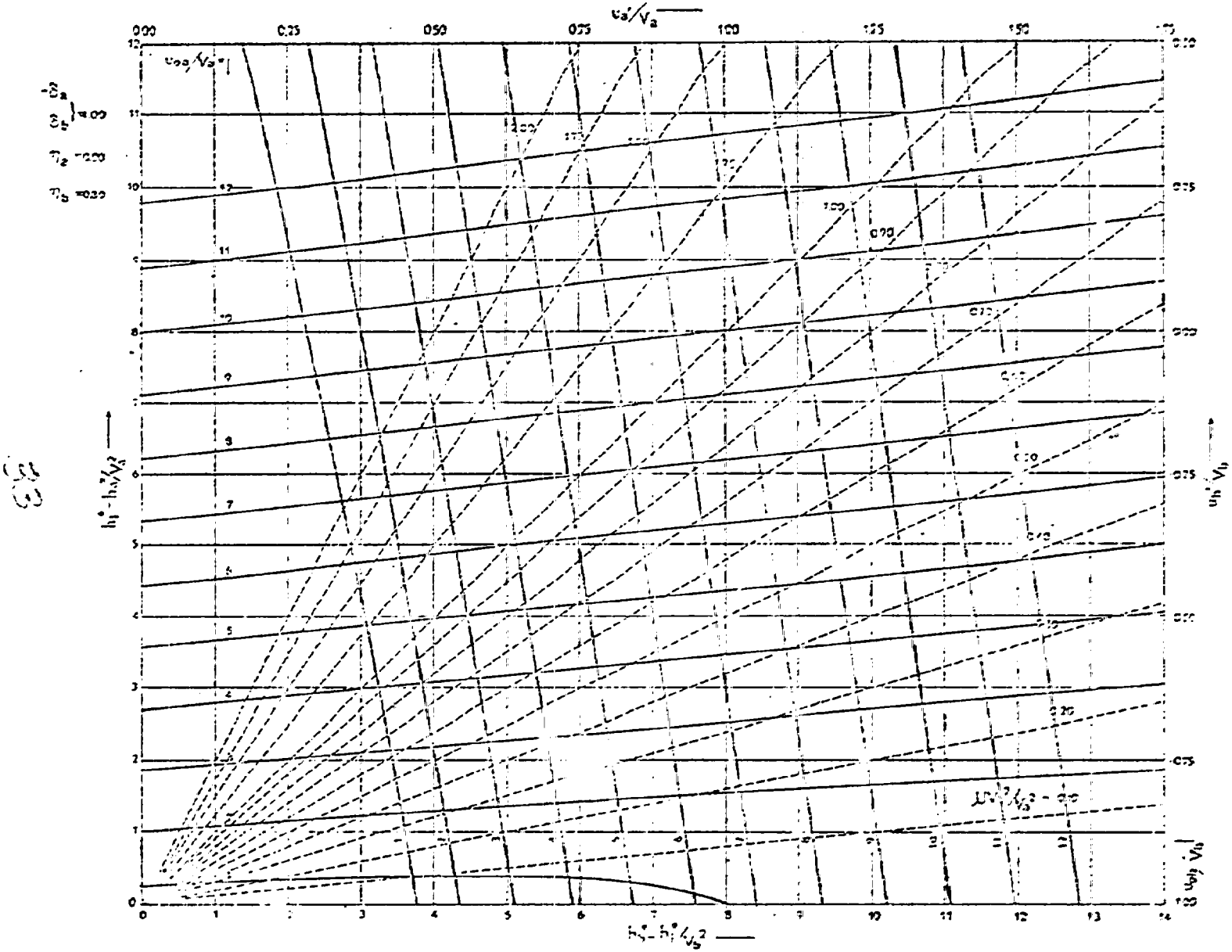
u_a/V_a
$-\delta_a$
δ_b = 0.00
η_a = 0.00
η_b = 0.20
u_{ab}/V_a = 1
$h_1^* - h_1^2/V_a^2$
$h_2^* - h_2^2/V_b^2$
u_b/V_b
$\Delta h^2/V_b^2$ = 0.00

FIGURE 3(f)

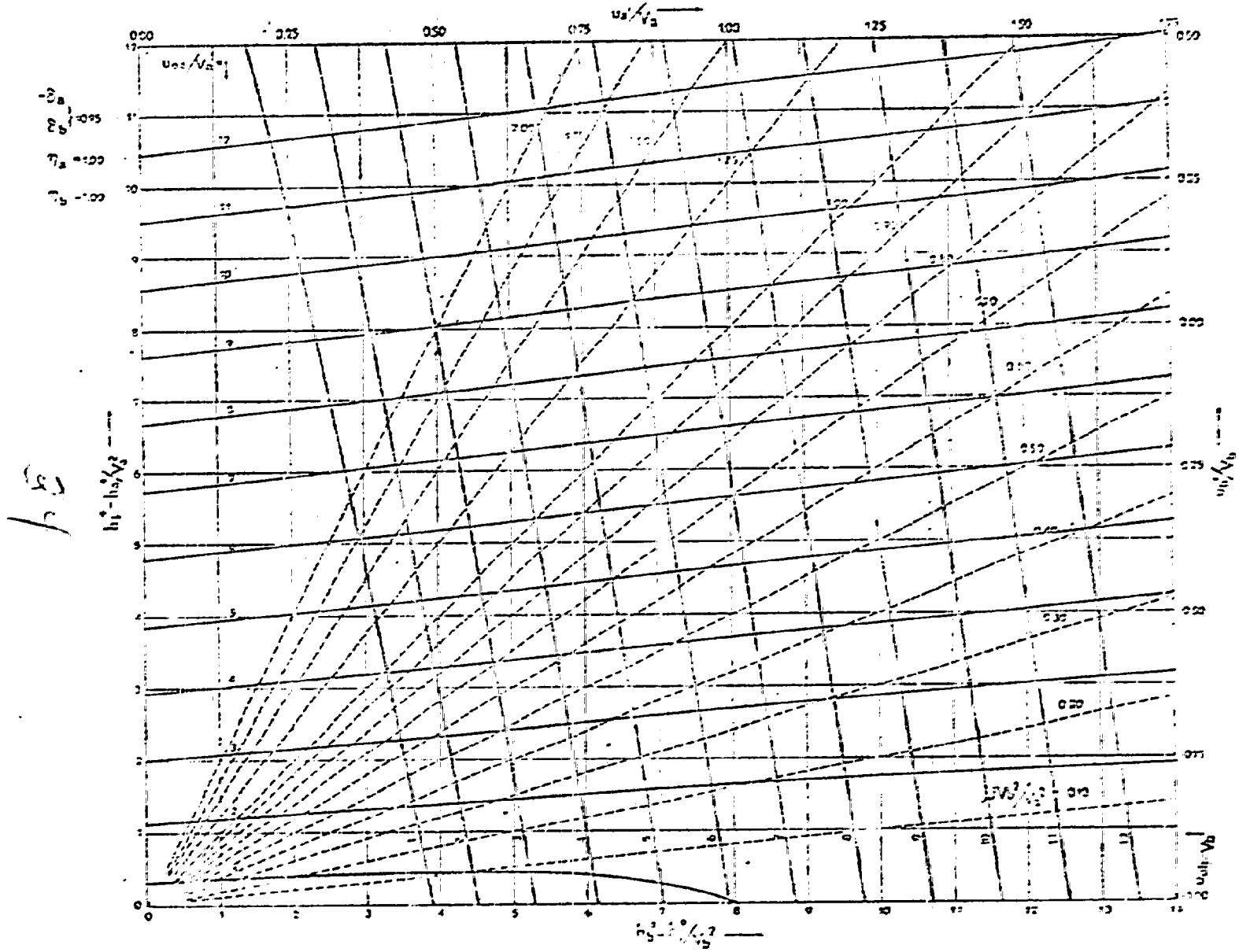

FIGURE 8(g)

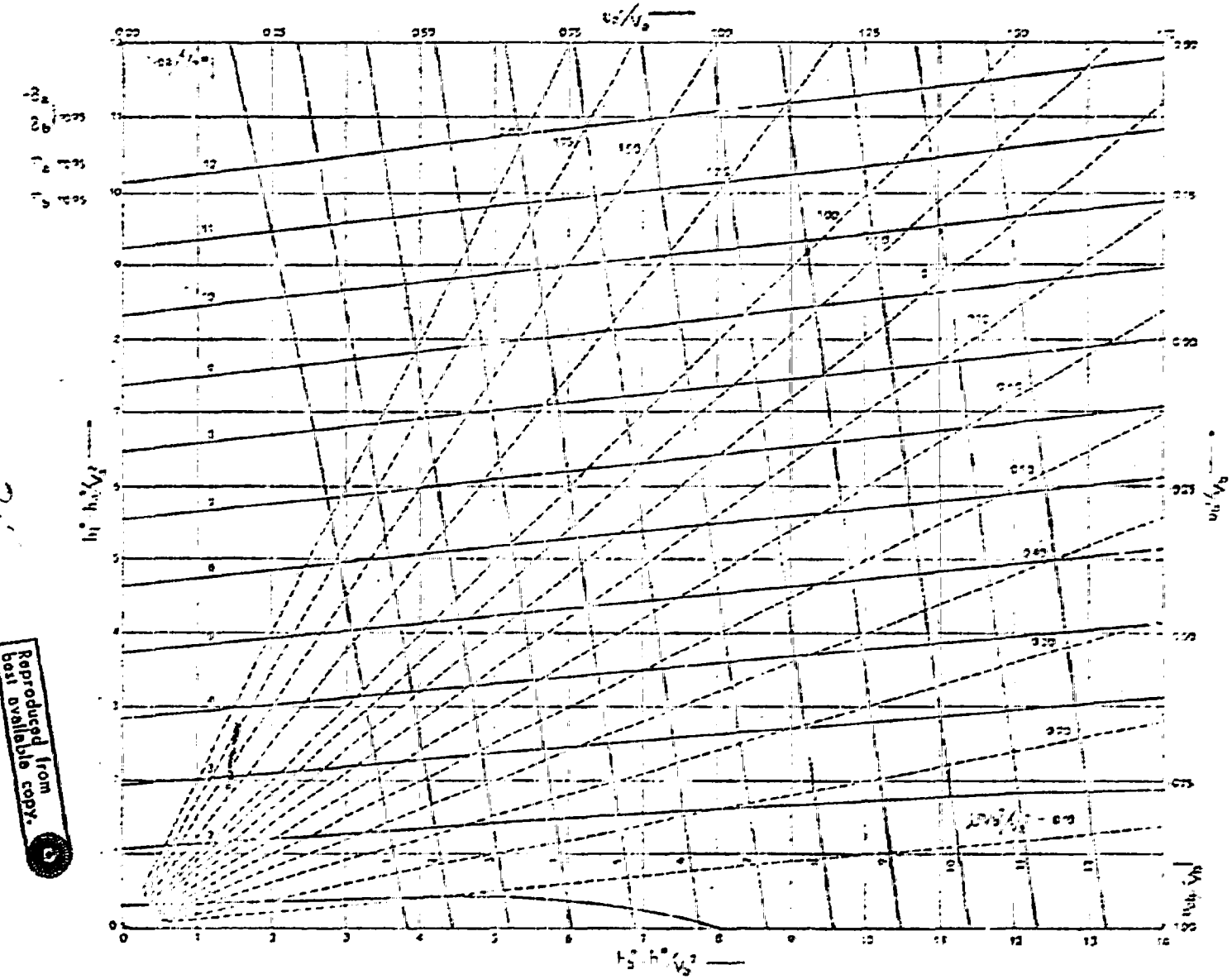

FIGURE 8(b)

(U) 3 FIGURE

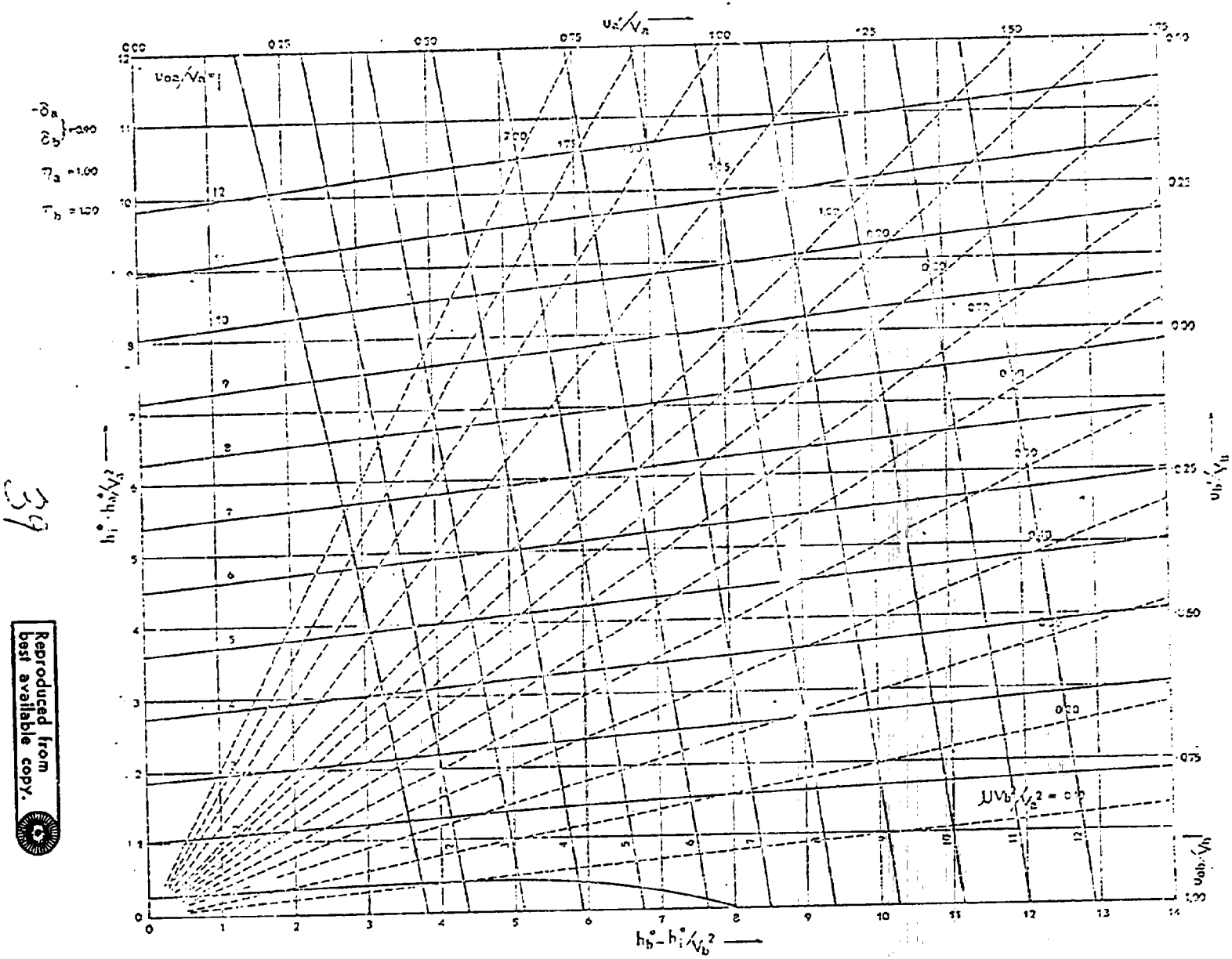

FIGURE 8(1)

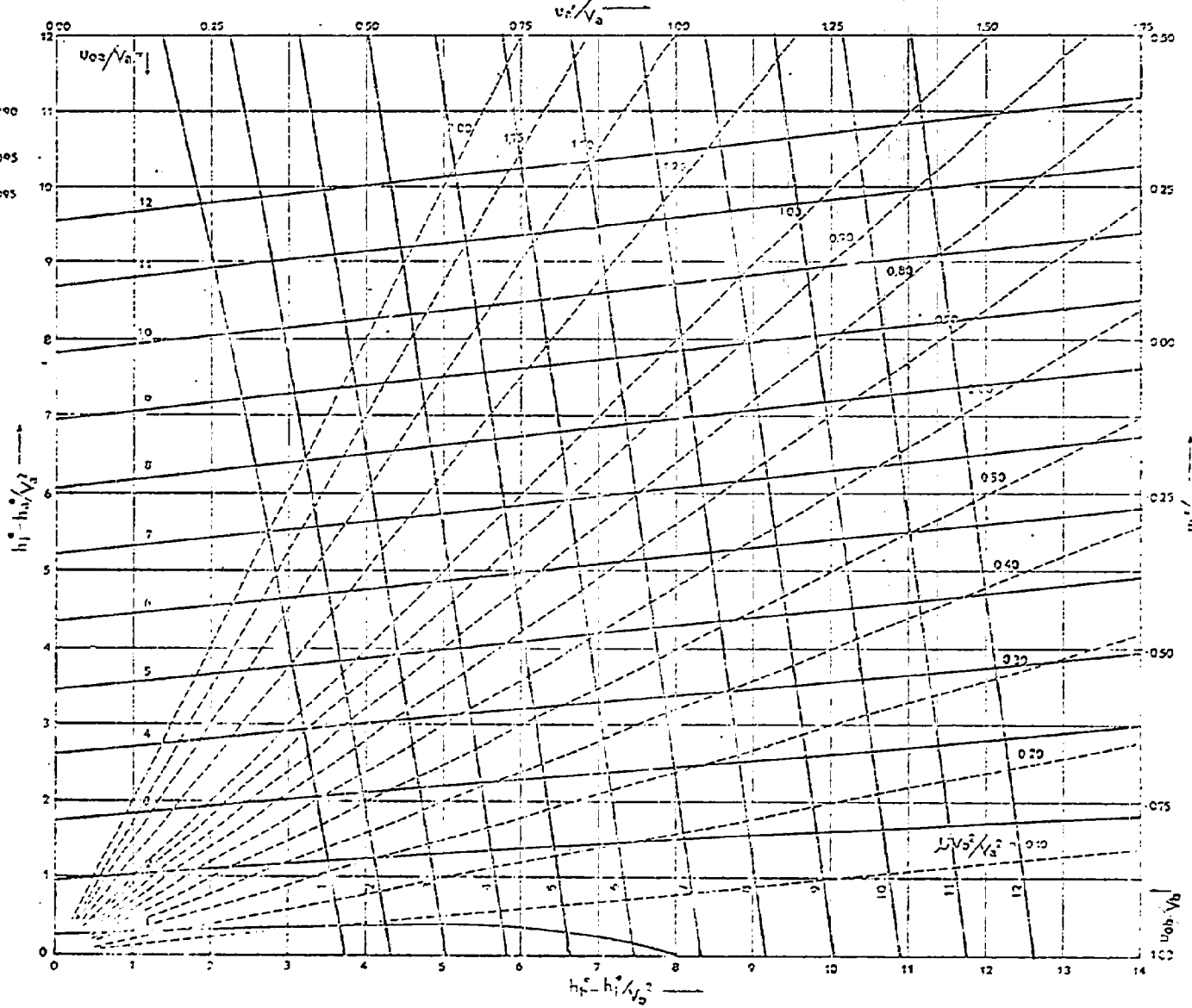

FIGURE 8 (--)

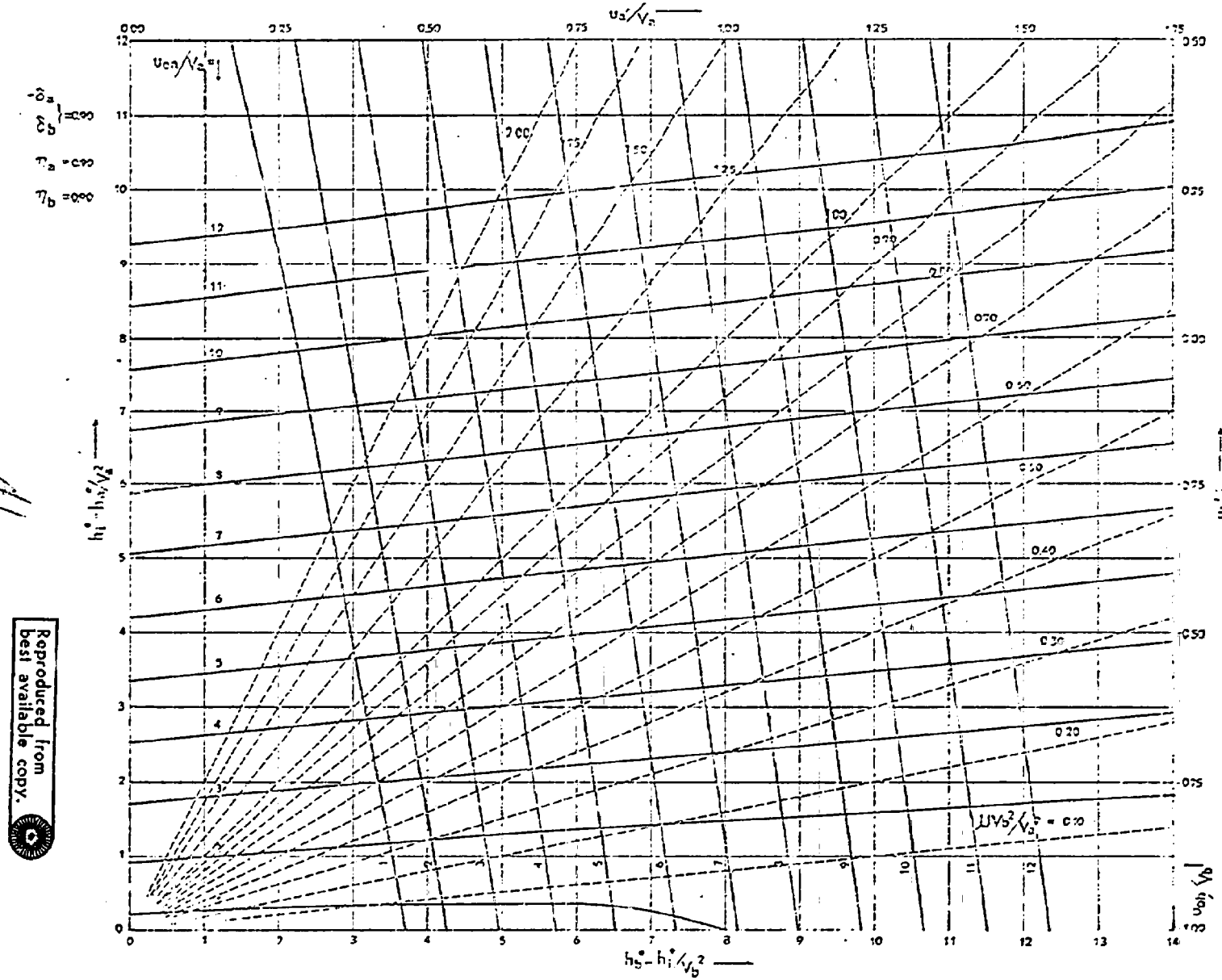

FIGURE 8(a)

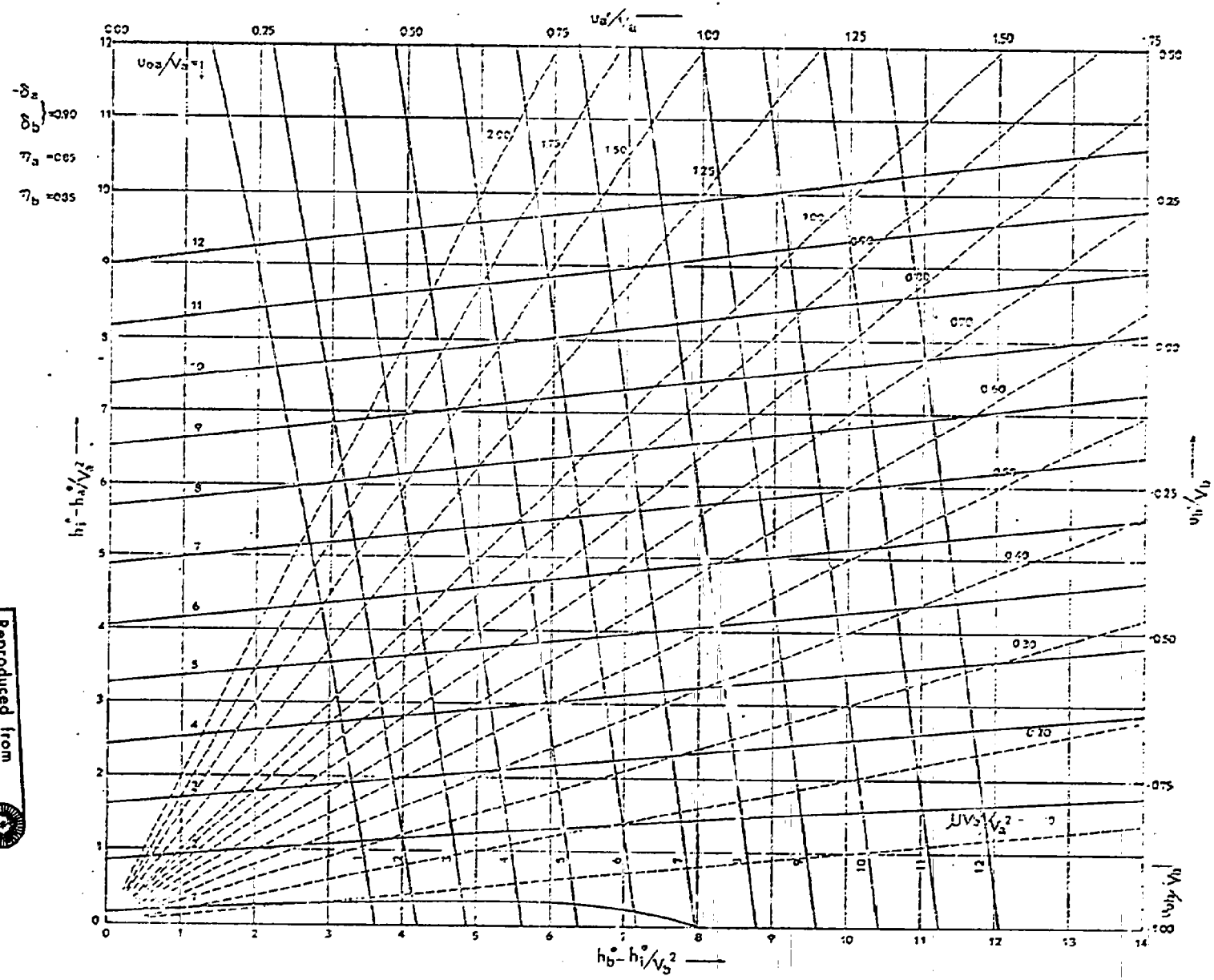

FIGURE 8 (c)

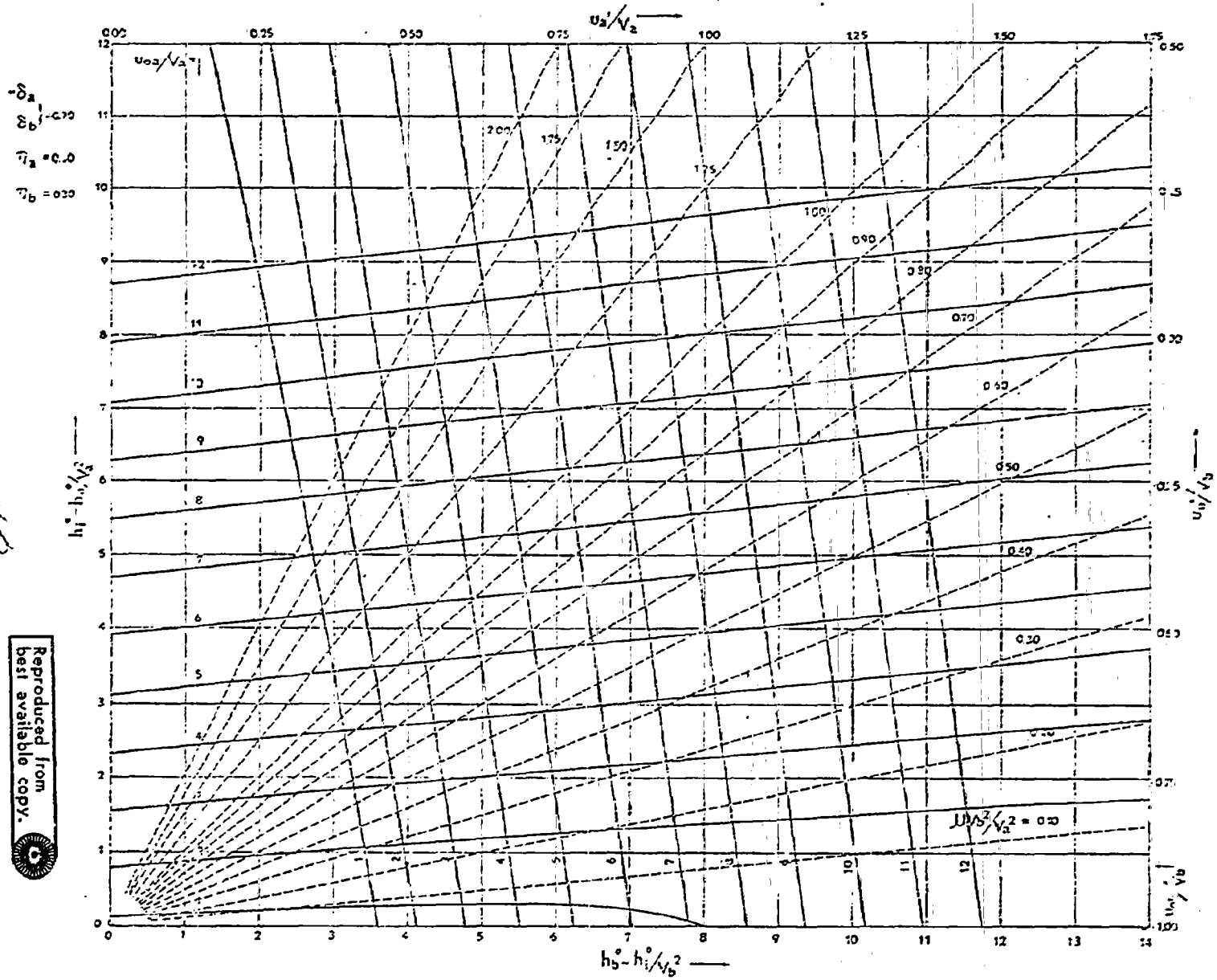

FIGURE 8(b)

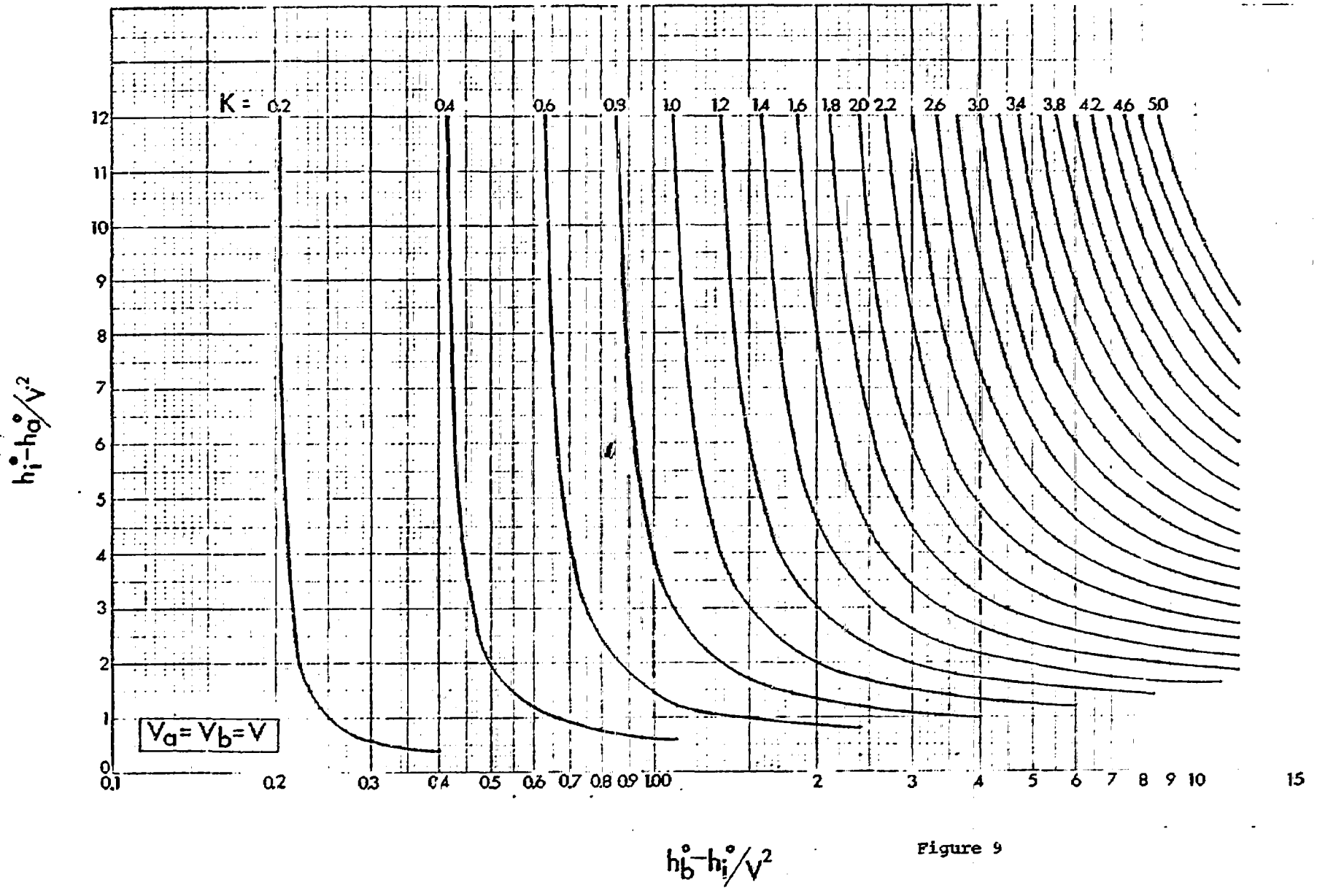
K = 0.2
0.4
0.6
0.8
1.0
1.2
1.4
1.6
1.8
2.0
2.2
2.6
3.0
3.4
3.8
4.2
4.6
5.0
$V_a = V_b = V$
$h_i^\circ - h_a^\circ / V^2$
$h_b^\circ - h_i^\circ / V^2$

Figure 9